Rapid Communications

Theory of polaritonic quantum-vacuum detection

Frieder Lindel,[1] Robert Bennett,[2] and Stefan Yoshi Buhmann[1]
[1]*Physikalisches Institut, Albert-Ludwigs-Universität Freiburg, Hermann-Herder-Straße 3, 79104 Freiburg, Germany*
[2]*School of Physics and Astronomy, University of Glasgow, Glasgow G12 8QQ, United Kingdom*

(Received 27 January 2020; accepted 28 September 2020; published 19 October 2020)

Recent progress in electro-optic sampling has allowed direct access to the fluctuations of the electromagnetic ground state. Here, we present a theoretical formalism that allows for an in-depth characterization and interpretation of such quantum-vacuum detection experiments by relating their output statistics to the quantum statistics of the electromagnetic vacuum probed. In particular, we include the effects of absorption and dispersion. Our results agree with available experimental data while leading to significant corrections to previous theoretical predictions and generalizing them to new parameter regimes. We show that transverse (free-field) as well as longitudinal (matter or near-field) fluctuations can be accessed individually by tuning the experimental parameters.

DOI: 10.1103/PhysRevA.102.041701

Over 90 years ago, Heisenberg formulated the uncertainty principle [1]. As one of its most fascinating consequences the commutation relations in quantum electrodynamics (QED) imply zero-point fluctuations of the electromagnetic field even in the quantum vacuum. Indirect evidence for these fluctuating fields can be seen in experiments measuring spontaneous decay rates [2], the Lamb shift [3], or the Casimir force [4]. These effects play an important role in many different areas of science, such as nanotechnology [5] and adhesion [6]. Recently, experiments based on nonlinear optics have opened up an alternative route to the ground state of the electromagnetic field [7,8]. In nonlinear optics photons can effectively be made to interact with each other [9–11], which has become an integral component of a wide range of experimental techniques [12–14] and permits remarkable insights into fundamental physics [15,16]. These new experimental techniques include electro-optic sampling [7,8] with a nonlinear crystal or the use of a time-dependent refractive index (the dynamical Casimir effect) [17,18].

In electro-optic sampling, a linearly polarized, ultrashort laser pulse propagates through a nonlinear crystal which mixes the laser pulse with any ambient electric field via its nonlinear properties [9]. This leads to a change of the pulse's polarization so that one obtains information about the ambient field inside the crystal [19,20]. The sensitivity of this setup to extremely weak electric fields provides direct access to zero-point fluctuations [7,21]. Using two such laser pulses (see Fig. 1), it is possible to retrieve information about correlations of the QED vacuum between distinct spatiotemporal regions [8], for example.

Following the pioneering works using such setups [7,8,20,22] and the accompanying theoretical analyses [21,23–25], the question regarding the nature of the quantum fluctuations accessed has been raised [26]. In particular, as electro-optic sampling is necessarily carried out inside a nonlinear optical crystal, the relation of the sampled quantum vacuum to the paradigmatic free-space vacuum is an important question. Here, we address this issue and offer a general theoretical framework based on macroscopic QED [27,28] which provides a basis for a detailed characterization and interpretation of quantum-vacuum detection via electro-optic sampling. Our theory is capable of predicting the output statistics of such experiments, accounting for inhomogeneous dispersive and absorptive media by considering the full medium-assisted ground state of the system as predicted by linear QED consisting of composite (polaritonlike) matter and free-field fluctuations—the vacuum which is probed is the *polaritonic* vacuum which generalizes the free-space vacuum to account for the nonlinear-crystal environment.

Polaritonic matter-field states have recently been studied in a variety of contexts. In photonic [29] and polaritonic Bose-Einstein condensates [30], the matter-field ground state emerges as a macroscopically occupied spatial mode of lowest energy. In the emerging field of polaritonic chemistry [31], molecules and solids of increasing complexity form polaritonic states inside cavities, significantly altering their physical and chemical properties.

Our formalism allows for studying of the rich ontological and spatiospectral structure of polaritonic quantum vacuum. We show that by tuning the parameters of the experimental setup within a realistic range, one can individually address longitudinal near-field fluctuations generated by the charges of the crystal and fieldlike propagating transverse ground-state fluctuations. In addition, our formalism overcomes the limitations of the paraxial approximation which is crucial to achieve good agreement with experimental data.

We begin with a brief account of the underpinnings of our theory. The propagation of a coherent laser pulse through a medium with second-order nonlinearity induces a nonlinear polarization field given by [9] $\hat{\mathbf{P}}_{\mathrm{NL}}(\mathbf{r},\omega) = \int_{-\infty}^{\infty} d\Omega\, \chi^{(2)}(\mathbf{r},\Omega,\omega-\Omega) \star \hat{\mathbf{E}}(\mathbf{r},\Omega)\hat{\mathbf{E}}(\mathbf{r},\omega-\Omega)$. Here, $\chi^{(2)}$ is the nonlinear susceptibility tensor of the medium, we use the convention $\hat{\mathbf{E}}(\mathbf{r},t) = \int_0^{\infty} d\omega\, \hat{\mathbf{E}}(\mathbf{r},\omega)e^{-i\omega t} + \mathrm{H.c.}$, and

$(\chi^{(2)}\star\hat{\mathbf{E}}\hat{\mathbf{E}})_i \equiv \sum_{jk}\chi^{(2)}_{ijk}\hat{E}_j\hat{E}_k$. The nonlinear polarization acts as an additional source term in the wave equation for the electric field, which can be formally solved as a Lippmann-Schwinger equation

$$\hat{\mathbf{E}}(\mathbf{r},\omega) = \hat{\mathbf{E}}_{\rm vac}(\mathbf{r},\omega) + \mathbf{E}_{\rm p}(\mathbf{r},\omega) + \mu_0\omega^2\int_{V_{\rm C}} d^3r'\,\mathbf{G}(\mathbf{r},\mathbf{r}',\omega)\cdot\hat{\mathbf{P}}_{\rm NL}(\mathbf{r}',\omega), \quad (1)$$

where μ_0 is the vacuum permeability, $\mathbf{G}(\mathbf{r},\mathbf{r}',\omega)$ is the Green's tensor of the vector Helmholtz equation [32], and $V_{\rm C}$ is the volume of the nonlinear crystal. In the vacuum picture, the coherent laser pulse is given by the sum of the vacuum field operator $\hat{\mathbf{E}}_{\rm vac}(\mathbf{r},\omega)$ and a classical laser pulse $\mathbf{E}_{\rm p}(\mathbf{r},\omega)$ [33]. Note that $\mathbf{E}_{\rm p}(\mathbf{r},\omega)$ may represent two spatially and temporally separated laser pulses, such as those featuring in the recent experiment [8]. To obtain the statistical properties of $\hat{\mathbf{E}}_{\rm vac}$ one could rely on microscopic models [34]. Here, we use the equivalent, but more general macroscopic QED which instead characterizes the polaritonic quantum vacuum inside the crystal via its linear permittivity, the classical Green's tensor, and polaritonic creation and annihilation operators $\hat{\mathbf{f}}^{(\dagger)}$, i.e.,

$$\hat{\mathbf{E}}_{\rm vac}(\mathbf{r},\omega) = i\frac{\omega^2}{c^2}\sqrt{\frac{\hbar\varepsilon_0}{\pi}}\int d^3r'\,\sqrt{{\rm Im}\varepsilon(\mathbf{r}',\omega)} \times\mathbf{G}(\mathbf{r},\mathbf{r}',\omega)\cdot\hat{\mathbf{f}}(\mathbf{r}',\omega). \quad (2)$$

The formal solution (1) for $\hat{\mathbf{E}}(\mathbf{r},\omega)$ is infinitely recursive. To solve it we use a Born series, which can be seen as a perturbation expansion in $\chi^{(2)}$ to the desired order. The zeroth-order contribution $\hat{\mathbf{E}}^{(0)}$ is given by the first line of Eq. (1) and the ith-order contribution reads

$$\hat{\mathbf{E}}^{(i)}(\mathbf{r},\omega) = -\sum_{j=1}^{i}\mu_0\omega^2\int_{V_{\rm C}} d^3r'\,\mathbf{G}(\mathbf{r},\mathbf{r}',\omega)\int_{-\infty}^{\infty}d\Omega\,\chi^{(2)}\star \times\hat{\mathbf{E}}^{(i-j)}(\mathbf{r}',\Omega)\hat{\mathbf{E}}^{(j-1)}(\mathbf{r}',\omega-\Omega). \quad (3)$$

This way, one obtains the electric field emerging from the nonlinear crystal as a function of the input fields and the Green's tensor.

We use our solution to Eq. (1) to find the output statistics of an electro-optic sampling experiment (see Fig. 1). These are found from the variance of the electro-optic operator $\hat{S}$, which for the single-beam setup used in Ref. [7] reads [21]

$$\hat{S} = \int_0^\infty d\omega\,A(\omega)\int d^2r_\parallel[i\hat{E}_y^\dagger(\mathbf{r}_\parallel,\omega)\hat{E}_x(\mathbf{r}_\parallel,\omega) + {\rm H.c.}], \quad (4)$$

where $A(\omega) = 4\pi\epsilon_0 cn(\omega)\eta(\omega)/\hbar\omega$, where η is the efficiency of the photodetector. For the more general setup used in Ref. [8] where two laser pulses $\mathbf{E}_{1,2}$ are used and which is also depicted in Fig. 1, one accesses the quantity $\hat{S}^2(\delta t,\delta\mathbf{r}_\parallel) = (\hat{S}_1\hat{S}_2+\hat{S}_2\hat{S}_1)/2$. Here, $\hat{S}_i$ is defined as in Eq. (4) but with the replacement $\mathbf{E}_{\rm p}\to\mathbf{E}_i$. Note that $\hat{S}^2(0,0)=\hat{S}^2$. Using the perturbation expansion outlined above up to second order in $\chi^{(2)}$ we can evaluate $\hat{S}^2(\delta t,\delta\mathbf{r}_\parallel)$ and find [32]

$$\langle:\hat{S}^2(\delta t,\delta\mathbf{r}_\parallel):\rangle = \int_0^\infty d\Omega\int_0^\infty d\Omega'\int_{V_{\rm C}}d^3r'\int_{V_{\rm C}}d^3r''\langle\hat{E}_{{\rm vac},x}(\mathbf{r}',\Omega) \times\langle\hat{E}^\dagger_{{\rm vac},x}(\mathbf{r}'',\Omega')\rangle F(\mathbf{r}',\mathbf{r}'',\Omega,\Omega')\rangle, \quad (5)$$

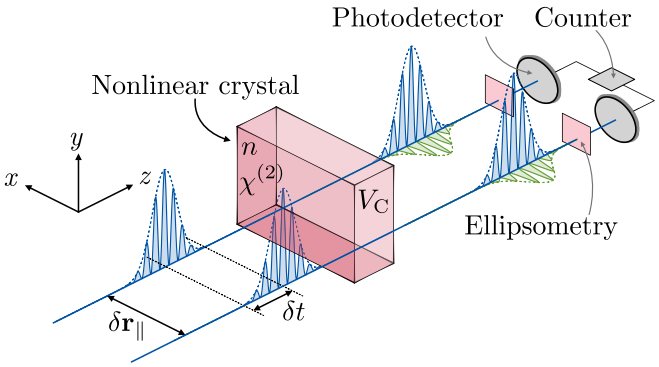

FIG. 1. Correlation measurement of the quantum vacuum via electro-optic sampling: Two linearly polarized laser pulses with mutual offset $\delta\mathbf{r}_\parallel$ and delay δt propagate through a nonlinear crystal with refractive index n, nonlinear susceptibility $\chi^{(2)}$, and volume V_C. The pulses mix inside the crystal via the nonlinear coupling with quantum fluctuations of the electromagnetic field, leading to a polarization shift of the laser pulses. Via an ellipsometry analysis of the emerging pulses from the crystal, it is possible to observe the quantum vacuum [8].

with the field correlation function given through macroscopic QED via Eq. (2) as [27,28]

$$\langle\hat{E}_{{\rm vac},x}(\mathbf{r}',\Omega)\hat{E}^\dagger_{{\rm vac},x}(\mathbf{r}'',\Omega')\rangle = \frac{2\hbar\mu_0}{\pi}\Omega^2\delta(\Omega-\Omega')\Big[\frac{1}{2}+n_T(\Omega)\Big]{\rm Im}[G_{xx}(\mathbf{r}',\mathbf{r}'',\Omega)], \quad (6)$$

where $n_T(\Omega)$ is the average thermal photon number at temperature T. The filter function F can be found in the Supplemental Material [32], and depends on the spatiotemporal probe beam profile, the relative spatial offset $\delta\mathbf{r}_\parallel$ and temporal delay δt, the optical and geometric properties of the crystal and its environment through the Green's tensor and the linear part of the crystal's permittivity, accounting for dispersion and absorption. It determines which spatial and spectral parts of the vacuum field are accessed via this quantum-vacuum detector (see Fig. 3). For a single laser pulse with a Gaussian profile and beam waist w, taken at equal frequencies and neglecting absorption, it reads [32]

$$F(\mathbf{r}',\mathbf{r}'',\Omega,\Omega) = \left(\frac{2|\chi^{(2)}|c\mu_0 N\omega_p}{{\rm w}^2 n}\right)^2 f(\Omega)^2 \times e^{-(\mathbf{r}_\parallel'^2+\mathbf{r}_\parallel''^2)/{\rm w}^2}e^{-in_g(\Omega/c)(z'-z'')} \quad (7)$$

(N, total number of detected photons; ω_p, average detected frequency; n, refractive index at the central frequency of the pulse $\omega_{\rm c}$; n_g, group refractive index; $f(\Omega)$, spectral autocorrelation function [21,32]).

The structure of Eq. (5) furnishes us with a clear physical picture for electro-optic sampling of vacuum fluctuations. The fluctuating electromagnetic fields inside the crystal (which cannot be directly detected by a photodetector) imprint their signature on the probe field. The ground-state correlation function of the electric field is hence sampled in a confined spatial region and a certain frequency interval defined by the spectral and spatial profile of the probe. Which part of the

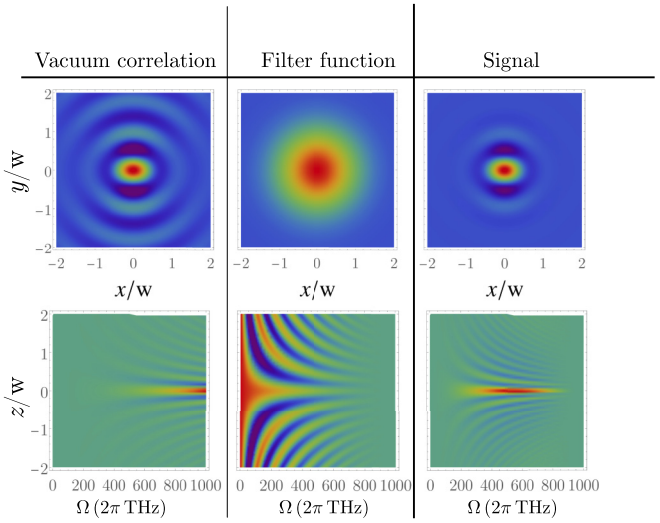

FIG. 2. Distinguishing contributions from the vacuum and from the filter function: We consider one y polarized laser pulse with Gaussian beam profile with beam waist $\mathrm{w} = 3\ \mu$m and duration $\Delta t = 5.9$ fs to propagate through a ZnTe crystal with length $L = 7\ \mu$m [32]. Using Eqs. (5)–(7) we plot the normalized filter function $F(\mathbf{r}, \mathbf{r}', \Omega)$, ground-state correlation function $\langle \hat{E}_{\mathrm{vac},x}(\mathbf{r}, \Omega)\hat{E}^{\dagger}_{\mathrm{vac},x}(\mathbf{r}', \Omega)\rangle$, and signal density $s^2(\mathbf{r}, \mathbf{r}', \Omega)$ defined by $\langle : \hat{S}^2 : \rangle = \int d\Omega \int d^3r \int d^3r' s^2(\mathbf{r}, \mathbf{r}', \Omega)$ for two different cases: In the first row we plot them as functions of x and y by setting $z = z' = \mathbf{r}'_{\parallel} = 0$ and $\Omega = 300 \times 2\pi$ TH, whereas in the second row we set $\mathbf{r}_{\parallel} = \mathbf{r}'_{\parallel} = z' = 0$ such that the only free variables are z and Ω.

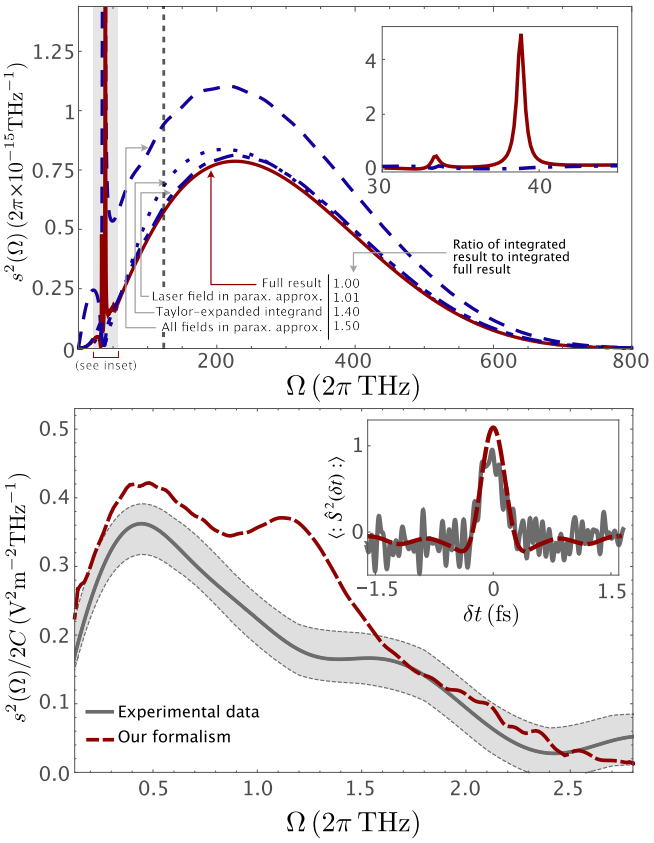

FIG. 3. Vacuum fluctuations in a bulk medium. Upper plot: We plot $s^2(\Omega)/N^2$ without approximations ("Full result"), and in the different various approximations: laser paraxial, Taylor expanded integrand, and the paraxial approximation. Note that we have simplified the numerics by replacing the full simulation with the laser paraxial approximation in the frequency range $\Omega < 50 \times 2\pi$ THz, where the two are indistinguishable in the absence of absorption. The cutoff discussed in the main text is shown by the dashed vertical line. Lower plot: We plot the signals spectrum $s^2(\Omega)$ normalized by $\sqrt{C} = 2\chi^{(2)}L\omega_p N/n\epsilon_0 c$, which is obtained from $\langle : \hat{S}^2(\delta t) : \rangle$ shown in the inset via a Fourier transformation. The experimental data and its standard deviation taken from Ref. [8] are shown in gray. Note that we used a different convention for the Fourier transform in order to obtain the spectrum from the time domain data compared to Ref. [8].

correlation function is accessed can be adjusted by tuning the experimental parameters such as the pump pulse profile or properties of the crystal which in turn determine the filter function, as shown in Fig. 2. This flexibility means that electro-optic sampling represents a much more versatile experimental route to accessing the quantum ground state of the medium-assisted electromagnetic field compared to more well-established methods such as the Purcell effect (which only accesses the two-point correlation function in the coincidence limit) or the Casimir force (to which all frequencies contribute). Since we left the laser pulse profile and the electromagnetic environment of the crystal unspecified and included absorption effects, Eq. (5) can be used as a starting point for studying the structure of the medium-assisted quantum vacuum in general absorptive and dispersive environments targeted at chosen spectral and spatial regions. This allows one to study the polaritonic nature of the electromagnetic ground state inside the crystal with unprecedented versatility. Note, however, that as for other methods of accessing the quantum vacuum, electro-optic sampling experiments can alternatively and equivalently be described in terms of radiation reaction [35]. Such an approach can, for example, predict Casimir forces without any reference to vacuum fluctuations of the electromagnetic field at all [36], instead considering a microscopic picture relying on correlated fluctuations of the atomic systems making up each plate. In electro-optic sampling, the corresponding microscopic picture consists of correlated up- and down-conversion processes, which can themselves be described by radiation reaction [37,38].

Our results generalize the theoretical framework previously obtained in Ref. [21] by including matter fluctuations in the quantum ground state and the effect of absorption on field propagation, and by allowing for arbitrary pulse profiles; by going beyond the paraxial approximation. In the limit of a Gaussian pulse profile, no absorption, and the paraxially approximated laser and vacuum fields, we recover the result of Ref. [21]. The latter is achieved by taking $k(\omega) \gg 1/\mathrm{w}$, then $q(\Omega) \gg 1/\mathrm{w}$, where $k(\omega)$ and $q(\Omega)$ are the wave vectors of the laser and the vacuum fields, respectively. The most dominant consequence of relaxing this last assumption is that, in that case, our theory is capable of including off-axis phase matching; using a $(2+1)$-dimensional Weyl decomposition, we find that in the phase-matching factor $\mathrm{sinc}[L\Delta k]$ with

$\Delta k = n_g\Omega/c - q$ the wave vector of the quantum fluctuations q is replaced by its z component $\sqrt{q^2 - q_x^2 - q_y^2}$. In order to assess the validity of the different approximations we use the same parameters as in Ref. [21] (also listed in the Supplemental Material [32]), which were in turn realized experimentally in Ref. [7]. The result for the integrand $s^2(\Omega)$ defined by $\langle :\hat{S}^2: \rangle = \int_0^\infty d\Omega\, s^2(\Omega)$ in the case of different approximations is shown in Fig. 3. We find that in this parameter regime absorption can be neglected, since the frequency of the only relevant material resonance is well below the most relevant frequency range sampled in the experiment. However, while the result with the paraxial approximation applied to the laser field agrees reasonably well with the full result obtained by direct evaluation of Eq. (5), not applying the paraxial approximation to the vacuum field reduces the signal by 50%, which is mainly due to unfavorable off-axis phase-matching conditions. Note that when following the suggestion of the authors of Ref. [21] of using a cutoff of the signal's spectrum at $n(\Omega)\Omega < c\pi/\mathrm{w}$, the predicted integrated signal differs from our more complex theory by 12%. A good tradeoff between simplicity of expression and inclusion of all relevant physical effects is found by Taylor expanding the integrand to find a next-to-leading order paraxial approximation applied to the vacuum field which agrees with the full result to around 6% [32].

Next, we turn our attention to the parameter regime exploited in Ref. [8] where two spatially and temporally separated laser beams are used. Again, we can derive a filter function from first principles for this experimental setup using Eq. (1) as a starting point. The derivation and the resulting expression together with the parameters under consideration can be found in the Supplemental Material [32]. Strikingly, by using two laser beams one can make a correlation measurement of the polaritonic ground state between different spatiotemporal regions, allowing one to obtain the spectrum $s^2(\Omega)$ by Fourier transforming the measured signal $\hat{S}^2(\delta t)$ [8], i.e., $1/(2\pi)\int_{-\infty}^{\infty} d\delta t\, \langle :\hat{S}^2(\delta t):\rangle e^{i\delta t\Omega} = \frac{1}{2}s^2(|\Omega|)$ [32]. In the parameter regime used in Ref. [8], which is also summarized in the Supplemental Material [32], we find that one can neither neglect absorption nor apply the paraxial approximation to the fluctuating field, but only the laser paraxial approximation applies. Neglecting absorption would lead to an additional unphysical peak of the signal around 2.25 THz, which has been avoided in the analysis of Ref. [8] by using a heuristic high-frequency cutoff. The result for the spectrum is compared to the experimental data in Fig. 3.

We find reasonable agreement between experiment and theory considering the errors on the input parameters. Note that our theoretical prediction does not contain *any* fitting parameter but is based on independently measured optical properties such as the linear and nonlinear response of the crystal. Also note that in this parameter regime, one mainly accesses thermal fluctuations and not zero-point ones, but these are treated on an equal footing in our generalized theory.

Having validated our theoretical approach we can now use it to gain a more fundamental insight into the nature of the quantum vacuum inside the crystal. The ground state inside the crystal is that of the coupled system of the electromagnetic field and the charges. Hence, the ground-state fluctuations consist of both fieldlike propagating fluctuations and the near field generated by the fluctuating charges inside the crystal. Note that the latter is not the same as the fluctuating field in empty space, but its generalization in the presence of an absorbing background medium, the photonlike part of the interacting system of photon and charges. It is well known (see, e.g., Ref. [39]) that in Coulomb gauge one can distinguish the two different types of contributions to the quantum vacuum of the electromagnetic field by decomposing the electric-field operator into its longitudinal ($\parallel$) and transverse ($\perp$) components [40]. Using this in Eq. (5), we find contributions to the signal's variance stemming from transverse and longitudinal fluctuations allowing one to analyze which of the two is accessed in the experiments. We use the same parameters as in Refs. [7,21] except that we vary the pulse duration Δt as shown in Fig. 4. We find that in the parameter regime of Refs. [7,21] where $\Delta t = 5.9$ fs, only transverse and hence fieldlike propagating fluctuations contribute to the signal, and the detected fluctuating field is dominated by photonlike fluctuations. Since the longitudinal part is proportional to $\mathrm{Im}(\varepsilon)$ [32], this can be understood from the fact that the main frequency range which is resolved is far from any material resonances [cf. Fig. 4(b)].

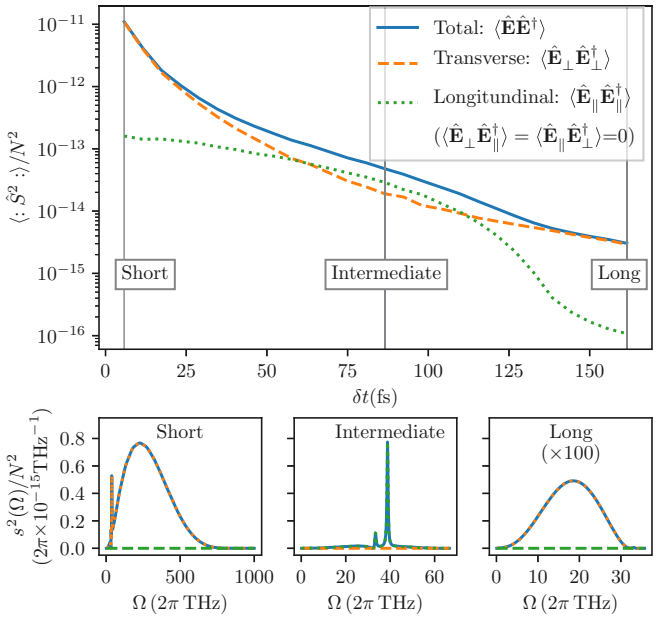

FIG. 4. Contribution to the variance for different pulse durations distinguishing longitudinal near-field and transverse propagating fluctuations: We see in (a) that there is an intermediate interval of Δt in which $\langle :\hat{S}^2: \rangle$ is dominated by longitudinal contributions. This can be explained by considering the spectra plotted for different values of Δt in (b), (c), and (d) as explained in the main text.

The situation changes for an intermediate pulse duration, where the resolved frequency range coincides with a material resonance [cf. Fig. 4(c)]. This leads to the detection of polaritonic modes which are dominated by their matter content resulting in mainly longitudinal fluctuations. For longer pulse duration, only field fluctuations spectrally far below the material resonance are detected, leading to a signal which

is dominated by transverse fluctuating fields as indicated in Fig. 4(d). This analysis reveals the possibility of unambiguously interpreting and identifying different properties of the richly structured polaritonic quantum vacuum inside the crystal using the formalism developed here.

In conclusion, we have outlined a theoretical framework for analyzing and interpreting the quantum-vacuum detector as provided by electro-optic sampling experiments sensitive to the QED vacuum. Our model includes absorption effects, goes beyond the paraxial approximation, and takes the full medium-assisted or polaritonic ground state into account. It agrees well with experimental data and offers significant improvements on previous theoretical works in an experimentally realized parameter regime. It also provides a detailed theoretical description which can be used to study, and perhaps reinterpret the conclusions of Ref. [7]. In addition, it provides a starting point for a detailed analysis of the polaritonic quantum vacuum and its rich structure in new, so far theoretically inaccessible, regimes. As an example, it was shown that transverse and longitudinal fluctuating fields can be analyzed individually, revealing the polaritonic nature of the QED ground state in media. This analysis applies more generally to photonic and polaritonic Bose-Einstein condensates and molecular polaritonic systems. Other characteristics of the quantum vacuum might be accessible using electro-optic sampling such as the influence of additional surfaces onto the electromagnetic ground state which is of relevance to, e.g., the Purcell or Casimir effect, or adhesion forces. Apart from electro-optic sampling, the general formalism resulting from our combining of macroscopic QED with nonlinear optics has applications in a wide range of fields such as recent studies of analogs of the dynamical Casimir effect [18], pair generation in ε-near-zero material or metamaterials [41], and photonic Bose-Einstein condensates [42].

The authors thank S. Barnett, T. Wellens, V. Shatokhin, G. Sorelli, N. Westerberg, C. Dittel, J. Faist, I.-C. Benea-Chelmus, F. F. Settembrini, D. Seletskiy, G. Burkard, and A. Leitenstorfer for fruitful discussions. R.B. acknowledges financial support by the Alexander von Humboldt Foundation, S.Y.B. acknowledges support from the Deutsche Forschungsgemeinschaft (Grant No. BU 1803/3-1476). R.B. and S.Y.B. both acknowledge support from the Freiburg Institute for Advanced Studies (FRIAS).

[1] W. Heisenberg, Z. Phys. **43**, 172 (1927).
[2] K. Drexhage, J. Lumin. **1-2**, 693 (1970).
[3] W. E. Lamb and R. C. Retherford, Phys. Rev. **72**, 241 (1947).
[4] H. B. G. Casimir, Proc. K. Ned. Akad. **360**, 793 (1948).
[5] F. M. Serry, D. Walliser, and G. J. Maclay, J. Appl. Phys. **84**, 2501 (1998).
[6] G. P. Brivio and M. I. Trioni, Rev. Mod. Phys. **71**, 231 (1999).
[7] C. Riek, D. V. Seletskiy, A. S. Moskalenko, J. F. Schmidt, P. Krauspe, S. Eckart, S. Eggert, G. Burkard, and A. Leitenstorfer, Science **350**, 420 (2015).
[8] I.-C. Benea-Chelmus, F. F. Settembrini, G. Scalari, and J. Faist, Nature (London) **568**, 202 (2019).
[9] R. W. Boyd, *Nonlinear Optics* (Academic, San Diego, 2003).
[10] S. Scheel and D.-G. Welsch, J. Phys. B: At., Mol. Opt. Phys. **39**, S711 (2006).
[11] D. E. Chang, V. Vuletić, and M. D. Lukin, Nat. Photonics **8**, 685 (2014).
[12] P. A. Franken, A. E. Hill, C. W. Peters, and G. Weinreich, Phys. Rev. Lett. **7**, 118 (1961).
[13] S. Mukamel, *Principles of Nonlinear Optical Spectroscopy* (Oxford University Press, New York, 1995).
[14] P. G. Kwiat, K. Mattle, H. Weinfurter, A. Zeilinger, A. V. Sergienko, and Y. Shih, Phys. Rev. Lett. **75**, 4337 (1995).
[15] M. E. Anderson, J. D. Bierlein, M. Beck, and M. G. Raymer, Opt. Lett. **20**, 620 (1995).
[16] C. Silberhorn, P. K. Lam, O. Weiß, F. König, N. Korolkova, and G. Leuchs, Phys. Rev. Lett. **86**, 4267 (2001).
[17] N. Westerberg, A. J. Prain, D. Faccio, and P. Öhberg, J. Phys. Commun. **3**, 065012 (2019).
[18] S. Vezzoli, A. Mussot, N. Westerberg, A. Kudlinski, H. D. Saleh, A. Prain, F. Biancalana, E. Lantz, and D. Faccio, Nat. Commun. Phys. **2**, 84 (2019).
[19] J. Valdmanis and G. Mourou, IEEE J. Quantum Electron. **22**, 69 (1986).
[20] C. Riek, D. V. Seletskiy, and A. Leitenstorfer, Eur. J. Phys. **38**, 024003 (2017).
[21] A. S. Moskalenko, C. Riek, D. V. Seletskiy, G. Burkard, and A. Leitenstorfer, Phys. Rev. Lett. **115**, 263601 (2015).
[22] C. Riek, P. Sulzer, M. Seeger, A. S. Moskalenko, G. Burkard, D. V. Seletskiy, and A. Leitenstorfer, Nature (London) **541**, 376 (2017).
[23] T. L. M. Guedes, M. Kizmann, D. V. Seletskiy, A. Leitenstorfer, G. Burkard, and A. S. Moskalenko, Phys. Rev. Lett. **122**, 053604 (2019).
[24] M. Kizmann, T. L. d. M. Guedes, D. V. Seletskiy, A. S. Moskalenko, A. Leitenstorfer, and G. Burkard, Nat. Phys. **15**, 960 (2019).
[25] A. S. Moskalenko and T. C. Ralph, Nature **568**, 178 (2019).
[26] A. Cho, Physicists observe weird quantum fluctuations of empty space—maybe, Science News: sciencemag.org, doi: 10.1126/science.aad4655 (2015, accessed 11.09.2019).
[27] S. Scheel and S. Y. Buhmann, Acta Phys. Slovaca **58**, 675 (2008).
[28] S. Y. Buhmann, *Dispersion Forces I: Macroscopic Quantum Electrodynamics and Ground-State Casimir, Casimir–Polder and van der Waals Forces* (Springer, Berlin/Heidelberg, 2012).
[29] J. Klaers, J. Schmitt, F. Fewinger, and M. Weitz, Nature (London) **468**, 545 (2010).
[30] J. Kasprzak, M. Richard, S. Kundermann, A. Baas, P. Jeambrun, J. M. J. Keeling, F. M. Marchetti, M. H. Szymanska, R. Andre, J. L. Staehli, V. Savona, P. B. Littlewood, B. Deveaud, and L. S. Dang, Nature (London) **443**, 409 (2006).
[31] J. Feist, J. Galego, and F. J. Garcia-Vidal, ACS Photonics **5**, 205 (2018).

[32] See Supplemental Material at http://link.aps.org/supplemental/10.1103/PhysRevA.102.041701 for derivations of Eqs. (5) and (6) as well as of the formulas and parameters used to generate Figs. 3 and 4. Also, an in-depth discussion of the origin of the fluctuations shown in the bottom part of Fig. 3 is included in it.
[33] P. L. Knight and L. Allen, *Concepts of Quantum Optics* (Pergamon, Oxford, 1983), p. 217.
[34] B. Huttner and S. M. Barnett, Phys. Rev. A **46**, 4306 (1992).
[35] J. Schwinger, *Particles, Sources and Fields* (CRC Press, Boca Raton, FL, 2018).
[36] J. Schwinger, Lett. Math. Phys. **1**, 43 (1975).
[37] T. J. Herzog, J. G. Rarity, H. Weinfurter, and A. Zeilinger, Phys. Rev. Lett. **72**, 629 (1994).
[38] P. W. Milonni, H. Fearn, and A. Zeilinger, Phys. Rev. A **53**, 4556 (1996).
[39] R. K. Bullough, J. Phys. A **2**, 477 (1969).
[40] T. G. Philbin, New J. Phys. **12**, 123008 (2010).
[41] A. Prain, S. Vezzoli, N. Westerberg, T. Roger, and D. Faccio, Phys. Rev. Lett. **118**, 133904 (2017).
[42] R. A. Nyman and M. H. Szymańska, Phys. Rev. A **89**, 033844 (2014).